

# Real-time noise cancellation with Deep Learning

Bernd Porr<sup>1</sup>, Sama Daryanavard<sup>1</sup>, Lucía Muñoz Bohollo<sup>1</sup>,  
Henry Cowan<sup>1</sup>, Ravinder Dahiya<sup>2</sup>

<sup>1</sup>Biomedical Engineering, James Watt School of Engineering, University of Glasgow, G12 8QQ, UK.

<sup>2</sup>Bendable Electronics and Sensing Technologies (BEST) group, James Watt School of Engineering, University of Glasgow, G12 8QQ, UK.

March 23, 2022

## Abstract

Biological measurements are often contaminated with large amounts of non-stationary noise which require effective noise reduction techniques. We present a new deep learning algorithm which performs real-time, continuous filtering of the data. As a poof of concept we demonstrate the algorithm's performance by reducing noise in electroencephalograms (EEG) with the help of a custom, flexible, 3D printed, compound electrode. With this setup an average of 4dB and maximum of 10dB improvement of the signal to noise ratio of the EEG was achieved by removing wide band muscle noise. This concept has the potential to not only improve the signal to noise ratio of EEG but can be applied to a wide range of biological, industrial and consumer applications such as industrial sensing or noise cancelling headphones. Keywords: Adaptive filters, noise

reduction, deep learning, EEG, smart electrodes, flexible electronics, bio-sensors.

## 1 Introduction

Low signal to noise (SNR) ratios exist in many application domains, such as communications, acoustics or biomedical engineering. In particular, the Electroencephalogram (EEG) (Green et al., 1985; Henry, 2006; Britton et al., 2016) has a low signal to noise ratio because of its low amplitudes, in the range of a few  $\mu V$ , which are contaminated from numerous sources, often orders of magnitude larger than the EEG signal itself (Jiang et al., 2019; Fatourehchi et al., 2007). In this work, we use EEG as an example application, however, the concept is not limited to this particular use case.

In order to increase the signal to noise ratio (SNR) of an EEG-signal one can divide the approaches into two categories: realtime processing and offline post-processing. With respect to the latter: by far the most popular offline approach is principle component analysis (PCA) or independent component analysis (ICA) (Jiang et al., 2019; McMenemy et al., 2010; Fitzgibbon et al., 2007; Delorme et al., 2007; Nordin et al., 2019). PCA and ICA first analyse the signals and then separate signal and noise. This analysis is offline, requires the signal and noise relationships to be constant over time, and demands high computational power.

Real-time algorithms perform the filtering of the EEG signals as they arrive sample by sample and do not need offline analysis, for example, bandpass filters, the short time Fourier Transform or wavelet transform (Ahmadi et al., 2012; Jirayucharoensak et al., 2013, 2019). These techniques still require prior knowledge of the noise to be able to tune the filter parameters. However, muscle noise is non-stationary due to voluntarily and involuntarily contraction of surrounding facial muscles. A solution to this problem is real-time adaptive filtering in which the noise is removed by an adaptive algorithm (Widrow et al., 1975; Kher and Gandhi, 2016; He et al., 2004). Such algorithms can run in real-time and use additional electrodes to provide information about the noise.

In cases where EEG electrodes are placed on top of the head (i.e. around  $C_z$ ) one can assume that noise polluting the EEG originates from further afield and affects all electrodes in equal measure, while the EEG signals originate locally (Fitzgibbon et al., 2015). If one uses a 2<sup>nd</sup> auxiliary electrode measuring just the noise one can use its signal to subtract the noise from the main EEG electrode. The most popular design for such an auxiliary electrode is a ring shaped electrode around the main EEG electrode where the noise is simply subtracted and is called “Laplace operator” (Makeyev et al., 2016; Fitzgibbon et al., 2015; Garcia-Casado et al., 2019; Aghaei-Lasboo et al., 2020; Besio et al., 2006; Makeyev et al., 2016). While the idea of simply subtracting the noise is perfect in theory, in practice the relationship between the EEG generated in the brain and the resulting signals at the electrodes are complex and dynamic. This calls for a smart, compound electrode that implements an adaptive filter to continuously learn about the changing signal and noise conditions. In this paper we present the proof of concept for a novel, compound electrode which can be easily manufactured in combination with a new deep learning algorithm to adaptively remove the noise from the EEG. This is demonstrated below by the removal of wideband muscle (EMG) noise.

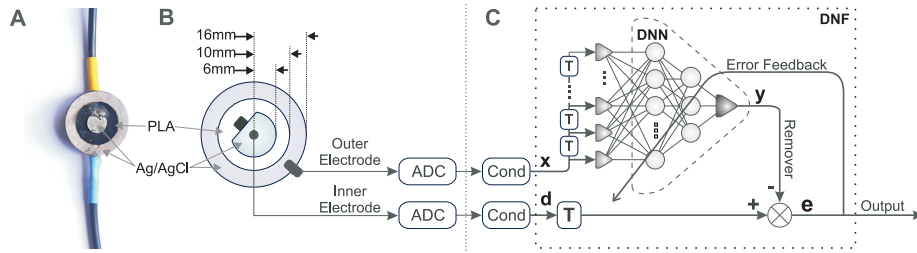


Figure 1: A) Photo of the manufactured compound electrode. The top wire (yellow) connects to the inner electrode, and the bottom wire (blue) to the outer electrode. B) Top schematic view of the new compound electrode showing the inner electrode and the outer electrode. C) Signal processing of the two signals originating from the inner and outer ring electrodes: ADC = Analogue Digital Converter, Cond = standard signal conditioning such as highpass filtering and 50Hz removal. T = time delay.

## 2 Methods

### 2.1 General signal requirements

Let us consider a signal  $\tilde{d}[n]$  measured with an ordinary electrode placed on the head of a subject:

$$\tilde{d}[n] = \underbrace{b[n] + m[n]}_{r[n]} + c[n] \quad (1)$$

which is a superimposition of three signals:

1.  $c[n]$  is the signal of interest generated by a stimulus or voluntarily, for example, in the setting of a brain computer interface (BCI),
2.  $b[n]$  is the background EEG activity which is involuntary and unaffected by the stimulus, and
3.  $m[n]$  is the accumulation of all artefacts, in particular muscle activity (EMG).  
The latter two signals form the total baseline noise  $r(n)$  contaminating the EEG component  $c[n]$  which is of interest for diagnostics or BCI applications.

The task is now to reduce  $r[n]$  as much as possible with the help of an opposing signal which ideally eliminates the noise from  $\tilde{d}[n]$ . As outlined in the introduction, we assume that the EEG originates *locally* from a small surface area of the head and that artefacts originate further afield and, therefore, they have a *global* and uniform strength across the head of the subject.

Naturally, a second and linearly independent measurement would provide more information about the relationship between the global noise and the local EEG signal. Consequently, a compound electrode (Fig. 1A,B) is designed with the addition of a larger ring-like outer electrode around the inner electrode, which acts as the noise reference. Thus, the compound electrode collects two separate signals:

$$\tilde{d}[n] = r[n] + c[n] \quad \text{Inner electrode: signal + noise} \quad (2)$$

$$\tilde{x}[n] = h[n] * (r[n] + \alpha c[n]) \quad \text{Outer electrode: noise reference} \quad (3)$$

where  $0 < \alpha \ll 1$  models the crosstalk between the inner  $\tilde{d}[n]$  and outer  $\tilde{x}[n]$  electrode signals because the signal  $c[n]$  of the inner electrode  $\tilde{d}[n]$  will also stray into the outer ring. The noise in turn should be present ideally in both the inner part of the electrode  $\tilde{d}[n]$  and the ring electrode  $\tilde{x}[n]$  but in practise it will be a filtered version and is modelled with the filter  $h[n]$ . The goal of the learning algorithm is to render the signal from the inner electrode  $\tilde{d}[n]$  as noise-free as possible so that ideally only  $c[n]$  remains. Naively, one could simply subtract the outer electrode signal  $\tilde{x}[n]$  from the inner one  $\tilde{d}[n]$  to obtain a noise free EEG but in practice this is not possible because of changing noise-characteristics which is modelled here with the filter  $h[n]$ . Instead, a new machine learning algorithm learns, in real-time, how to alter the signal from the outer noise reference electrode  $\tilde{x}[n]$  in a way that it eliminates the noise from the inner electrode which then results in a noise-free EEG signal. In the next two sections we describe first the electrode and then the deep neuronal filter algorithm.

## 2.2 Fabrication of the compound electrode

To record both the noisy EEG and a noise reference a new compound electrode was designed (Fig. 1A/B). The physical design of the electrode was driven by durability, ease of manufacture and reliability. Polylactate acid (PLA) was chosen as the electrode material due its compatibility, flexibility, and adhesive nature to silver/silver-chloride (Ag/AgCl) ink (Rohaizad et al., 2019). Ag/AgCl paste was selected for the conductive portion. The combination flexible backing with conductive paste versus conventional, rigid, often uncomfortable gold/platinum electrodes (Di Flumeri et al., 2019), (Lopez-Gordo et al., 2014), is advantageous as it allows a degree optimal skin-electrode via the flexion of the electrode on the contact area. This optimal contact also ensured minimal inter-electrode impedance resulting in an increased SNR for that electrode whilst also increasing the comfort for the patient

(Suarez-Perez et al., 2018) making long-term monitoring applications more viable. The compound electrode consists of two raised ring portions separated by a channel. The PLA geometry was 3D printed. The surface areas of the different electrode compounds were:

$$\begin{aligned}
 A_{InnerRing} &= \pi \times 6mm^2 = 113mm^2 \\
 A_{OuterRing} &= A_{Outside} - A_{Inside} \\
 A_{Outside} &= \pi \times 15mm^2 = 707mm^2 \\
 A_{Inside} &= \pi \times 10mm^2 = 314mm^2 \\
 A_{OuterRing} &= 530mm - 78mm \approx 393mm^2
 \end{aligned} \tag{4}$$

A layer Ag/AgCl paste was deposited on each of the raised rings using a plastic spatula. The Ag/AgCl was then cured at 70°C for 1 hour. Figure 1A shows the final printed electrode with Ag/AgCl applied. Wires were connected to the electrode substrate by melting the wires into the flexible PLA geometry using a soldering iron, then applying pure silver paste to ensure electrical contact, and epoxy to further solidify the connection. This electrode has proven to be robust and easy to both manufacture and integrate into a headband or EEG cap as a wearable device.

### 2.3 Experimental setup for EEG recording

Ethical approval for this experiment was obtained from the Glasgow University's research ethics committee. In total 20 subjects were recruited and each subject held two sessions with no intervals as to guarantee consistent electrode signals:

1. P300 visually induced oddball stimulus to determine the EEG signal  $c[n]$  (5 minutes). The subject had the task to count mentally the number of oddball stimuli. The sampling rate was  $f_s = 250$  Hz.
2. Contracting the jaw muscle every 15 secs to generate EMG noise. The sampling rate was  $f_s = 500$  Hz.

The data was acquired using an Attys device ([www.attys.tech](http://www.attys.tech)) and the data acquisition programs 'attys-ep' and 'attys-scope'. The Attys was connected to electrodes placed on the participant's head. Referring to the international 10-20 system, the compound electrode was placed at  $C_z$ , with the inner part connected to the positive input of Channel 1 and the outer ring electrode to Channel 2. The A2 electrode was connected to the negative input of Channel 1, and the A1 electrode was connected to ground.

## 2.4 Deep Neuronal Filter (DNF)

Fig. 1C shows the block diagram of our Deep Neuronal Network (DNN) which in conjunction with the additional building blocks becomes our novel Deep Neuronal Filter (DNF) to remove noise (see Daryanavard et al. 2022 for the source code). Recall that the deep network exploits the assumption that the signal from the outer electrode  $x[n]$  ideally just contains the noise and that the DNN learns to subtract it from the signal  $d[n]$  originating from the inner electrode at the summation node “X”. The teaching signal  $e[n]$  of the network is the actual output signal of the network as in any other standard noise cancellation frameworks, for example LMS filters. This means that the network will remove any noise from the outer electrode  $x[n]$  which is *correlated* with the noise from the inner electrode  $d[n]$ .

As with any neural network it will always try to learn the strongest correlation. However, eyeblink artefacts and slowly changing electrode drift have much higher signal power than EMG. Given that we are interested in EMG we need to provide the reference noise input  $x[n]$  with the muscle noise spectrum and removing the much more powerful, low frequency artefacts such as eye movement or baseline wander. We do this by employing a highpass filter which captures the typical EMG wideband spectrum. Here, we set the 2nd order Butterworth highpass to  $f_{c_x} = 5 \text{ Hz}$  which gives a shallow rolloff. The highpass filter frequency for the inner signal  $d[n]$  is not critical and was set to  $f_{c_d} = 0.5 \text{ Hz}$  to simply remove the DC from the DC coupled ADC converter so that all signals are DC free:

$$d[n] = \gamma \cdot \text{HP}_{f_{c_d}}[n] * \text{BS}[n] * \text{LP}_{\text{ADC}} * \tilde{d}[n] \quad (5)$$

$$x[n] = \gamma \cdot \text{HP}_{f_{c_x}}[n] * \text{BS}[n] * \text{LP}_{\text{ADC}} * \tilde{x}[n] \quad (6)$$

where  $\text{HP}_{f_{c_d}}[n]$  and  $\text{HP}_{f_{c_x}}[n]$  are the 2nd order highpass Butterworth filters for the inner and outer electrode respectively.  $\text{BS}[n]$  is a 2nd order Butterworth notch filter against powerline interference at 50 Hz.  $\text{LP}_{\text{ADC}}$  is the lowpass characteristic of the sigma delta converter with a cutoff at about half the sampling rate. The gain was set to  $\gamma = 1000$  so that each neuron in the input layer of the neural network received values of approximately  $\pm 0.2\text{V}$ .

Inspired by a Finite Impulse Response (FIR) filter, we send the signal of the outer electrode  $x[n]$  through a tapped delay line with

$$N_{\text{taps}_x} = \frac{f_s}{f_{c_x}} \quad (7)$$

taps and then feed it into the Deep Neural Network (see Fig. 1). The signal  $d[n]$  is delayed by  $N_{\text{taps}_x}/2$  so that the DNN has time to react to pulse-like muscle artefacts arriving at  $x[n]$ .

The output of the Deep Neural Network  $y[n]$  is then used to remove the noise from  $d[n]$ :

$$e[n] = d[n] - y[n] \quad (8)$$

which is then ideally the noise-free EEG which is at the same time the error signal for the DNN and back-propagated in real-time. Learning is “on” (i.e. in effect) at *all times*, meaning, the network adjusts to the changes in the electrode contact as they happen.

The network used for DNF is a feed forward neural network with fully connected layers designed with  $L = 6$  layers. The number of neurons  $I(\ell)$  per layer index  $\ell$  is calculated as:

$$\begin{aligned} b &= e^{\frac{\ln N_{\text{taps}_x}}{L-1}} \\ I(\ell) &= \frac{N_{\text{taps}_x}}{b^\ell} \end{aligned} \quad (9)$$

which guarantees that the output layer consists of exactly one neuron which then generates the “remover”  $y[n]$ . In our case with  $N_{\text{taps}_x} = 50$  inputs to the DNF this results to:  $I = 50, 22, 10, 4, 2, 1$  neurons per layer which means that the 1<sup>st</sup> layer is fully connected with the same number of neurons to the delay line and then the number of neurons are reduced in form of a funnel as done in auto-encoders.

The weights of the neurons were initialised to a random value in the range of  $(0, 1]$ . Eq.11 below shows the forward propagation of the outer electrode signal  $x[n]$  through the first layer of the network:

$$a_j^0[n] = \tanh(z_j^0[n]) = \tanh \left( \sum_{k=0}^{N_{\text{taps}_x}} (\omega_{kj}^0 x[n-k]) \right) \quad (11)$$

where  $x[n-k]$  is the filtered signal from the  $k^{\text{th}}$  tap of the delay line for the outer electrode signal (Fig.1). In contrast to deep networks performing classification we perform filtering of a DC free signal. For that reason there are no bias weights to keep the processing DC free. The activation function is  $\tanh$  because it is ideal for signal processing: it is linear at the origin and becomes non-linear with growing signal strength so that learning can self-tune the non-linear processing. In the frequency domain this means the network self-tunes the amount of harmonics it is

adding to the signals and thus to the remover  $y[n]$ .

Similarly, these activations propagate through the deeper layers in the network:

$$a_j^\ell[n] = \tanh(z_j^\ell[n]) = \tanh\left(\sum_{i=0}^{I(\ell)} \omega_{ij}^\ell a_i^{\ell-1}[n]\right) \quad \text{where: } \ell : 1, \dots, L-1 \quad (12)$$

Finally, in the output layer this weighted sum results in the generation of the ‘‘Remover’’ signal  $y[n]$ :

$$y[n] = \tanh(z_0^{L-1}[n]) = \tanh\left(\sum_{i=0}^{I(L-1)} \omega_i^{L-2} a_i^{L-2}[n]\right) \quad (13)$$

The remover signal  $y[n]$  then ideally cancels out the noise from the inner electrode  $d$ :

$$e[n] = d[n] - y[n] \quad (14)$$

As explained in the previous sections, the output of the DNF  $e[n]$  is the noise-free EEG signal and is also used for the learning of the neural network which is done by error backpropagation:

$$\delta^{L-1} = e[n] \quad (15)$$

where  $\delta^{L-1}$  is the error in the output neuron which is then backpropagated.

For deeper layers this is defined through the back-propagation as:

$$\delta_j^\ell = \sum_{k=1}^K (w_{jk}^{\ell+1} \delta_k^{\ell+1}) \cdot \tanh'(Z_j^\ell) \quad \text{where: } \ell : L-2, \dots, 0 \quad (16)$$

The changes in weights that cause the optimum reduction in noise is dictated by gradient descent rule:

$$\Delta\omega_{ij}^\ell = \eta a_i^{\ell-1} \cdot \delta_j^\ell \quad (17)$$

where  $\eta$  is the learning rate.

It's important to note that the effective learning rate  $\eta_e$  directly scales with the amplitude of the noise reference  $x[n]$ :

$$\eta a_i^{\ell-1} \cdot \delta_j^\ell \equiv \underbrace{\eta x[n]}_{\eta_e} \cdot e[n] \quad (18)$$

To have a constant effective learning rate one could either normalise the noise

reference  $x[n]$  or adjust the learning rate dynamically if the average amplitude of  $x[n]$  is changing. In this work we directly set the learning rates to accommodate the two different noise reference amplitudes of  $x[n]$  for the P300 task ( $\eta = 10$ ) and the jaw muscle task ( $\eta = 2.5$ ) so that the effective learning rates were the same between the two tasks. The above equation also shows that learning converges when the correlation between the noise reference  $x[n]$  and the error signal  $e[n]$  averages out, meaning no frequency components of the noise present in the outer electrode signal is remained in the output of the DNF filter and thus the noise has been removed.

## 2.5 Calculating the signal to noise ratio

The *signal* from the inner electrode (Eq. 2) is a mix of baseline EEG, EMG and the consciously created EEG signal  $c[n]$ . In order to have a realistic estimate of  $c[n]$  we use the power of the primary peak of the P300 evoked potential. To reduce the noise of the peak we took the median power between  $300\text{ ms} \dots 500\text{ ms}$  which takes into account the  $100\text{ ms}$  latency of the wireless transmission between the ADC and the P300 software. This means that in terms of the power of the signal we can think of the P300 of a pulse at  $t = 300\text{ms}$  which could be detected to, for example, setting up a P300 speller. Note that the median over this time interval will underestimate the power slightly. However, this is deliberate because realtime BCI systems will hardly average over 5 minutes (rather seconds), will deal with much lower signal strengths for  $c[n]$  and thus using the median filter corrects for an overly optimistic signal strength.

In terms of *noise* we are interested in the power of the EMG generated by facial muscles and the jaw muscle but not in the low frequency band such as electrooculogram (EOG) or electrode drift. To asses mainly EMG and underlying EEG background noise we calculated the periodogram with the Welch method which had a window length at the sampling rate giving the power density in bins of 1 Hz. The power density samples from  $5\text{ Hz} \dots 125\text{ Hz}$  were summed up given the total noise power in the frequency band between  $5\text{ Hz}$  and  $125\text{ Hz}$ .

The signal to noise ratio is then calculated as:

$$\text{SNR} = \frac{\text{median}(v_{P300, \pm 100\text{ms}}^2)}{\sum_{k=5\text{ Hz}}^{125\text{ Hz}} \text{Welch}(v)[k]} \quad (19)$$

where  $v$  can be one of the following signals: a) the inner electrode signal  $d[n]$ , b) the output  $e[n]$  of the DNF, c) the output of a standard FIR based LMS filter and d) the output of Laplace operator by directly subtracting the raw outer electrode

signal  $\tilde{d}[n]$  from the inner  $\tilde{x}[n]$  one.

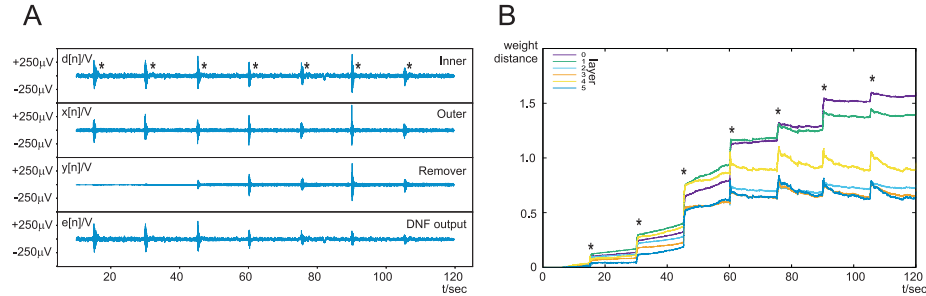


Figure 2: Signals and weight development from subject 10 while contracting their jaw muscles every 15 seconds. The jaw contractions are indicated with a “\*”. A) Four signal traces which are the inner electrode signal  $d[n]$  which carries a mix of EEG and EMG, the outer electrode signal  $x[n]$  which is the noise reference, the output of the DNN, the “remover”  $y[n]$ , and the output of the DNF  $e[n]$  which is both output and error signal. B) Weight development: shows the Euclidean weight distance from the initial weights of the 6 different layers over time.

### 3 Results

The data from the 20 subjects (Munoz Bohollo and Porr, 2022) were examined for electrode failure or strong external interference. Subject 2 had a faulty  $x[n]$  channel and subject 5 had unexplained strong artefacts possibly from a power surge. Thus, subjects 2 and 5 were excluded. Fig. 2A shows the progress of realtime learning of the DNF over a period of 2 mins for subject 10. “Inner” shows the signal  $d[n]$  of the inner part of the compound electrode. The voluntary jaw muscle contractions every 15 seconds are clearly visible and indicated with a “\*”. Between the muscle contractions the signal is most likely a mix of baseline EEG and lower amplitude involuntary facial muscle (EMG) activity. The “Outer” trace shows the signal from the outer ring electrode  $x[n]$  where the EMG bursts, caused by the jaw muscles, are clearly visible. These two signals, “Inner” and “Outer”, are then sent into the Deep Neuronal Filter (DNF). The most important internal signal is the “Remover”  $y[n]$  which eliminates the noise (Eq. 14). The result of the subtraction  $e[n]$  can be observed in the bottom trace “DNF output”.

The DNN has in total 6 layers and their weight development related to Fig. 2A is shown in Fig. 2B over the two minutes. Plotted is the weight distance from the initial randomly initialised weight values. Learning is fastest during the jaw

muscle contractions as the noise reference  $x[n]$  has a higher amplitude and thus the effective learning rate is higher (Eq. 18) during the jaw muscle bursts but also continues to learn between EMG bursts at a lower rate. From about 60 seconds learning has stabilised with only smaller adjustments to the weights till the end of the experiment. Because the filter acts in closed loop corrective action happen where the weights shrink again after a jaw contraction indicating that jaw muscle recruitment and involuntary muscle activity cause slightly different correlations so that the network re-adjusts.

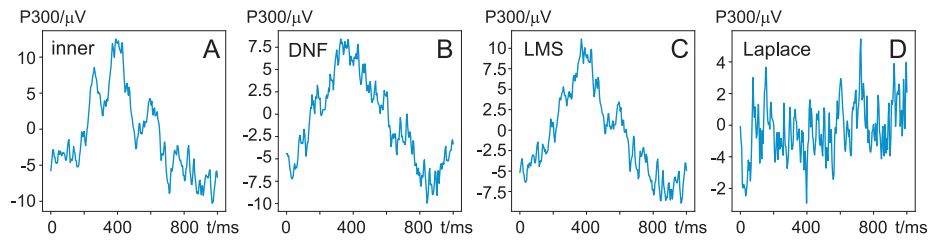


Figure 3: P300 averages from subject 10 who was presented with oddball stimuli randomly chosen every 8sec-13sec while looking at a chequer board which inverted every second. The recording was 5 minutes long. A) the event triggered average from the inner electrode  $d[n]$ , B) the event triggered average from the output  $e[n]$  of the DNF, C) the output from the LMS filter (adaptive FIR filter) and D) from the Laplace filter:  $\tilde{d}[n] - \hat{x}[n]$  with DC and 50 Hz removed after the subtraction operation.

In order to calculate the signal to noise ratio one needs to calculate the power of the signal and the power of the noise (see Eq 19). As outlined above the signal power is estimated by calculating the power of the primary P300 peak. Fig. 3 shows the P300 peaks just from the inner electrode (A), filtered by the DNF (B), filtered by a classical LMS FIR filter (C) and by the Laplace operator (D). Starting with (D) it is evident that the Laplace operator completely removes the P300 peak basically rendering the SNR calculations for a pure Laplace operator impossible. Comparing the P300 from the original electrode signal (A) with that of the DNF (B) output the P300 peak of the DNF is reduced by approximately 1/4 (from 10  $\mu\text{V}$  to 7.5  $\mu\text{V}$ ) while the LMS filter causes virtually no reduction. This means that the DNF filter needs to reduce the noise even more than the LMS to achieve an overall SNR improvement, as the DNF diminishes the P300 peak. However, this is expected as there is certainly crosstalk between the inner electrode and the outer ring electrode as mentioned before (Eq. 3).

Fig. 4A shows the power spectral density of the signal from the inner electrode

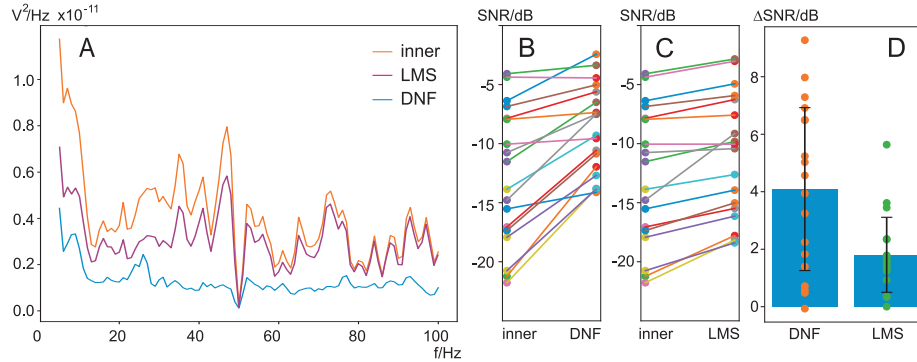


Figure 4: Noise density and signal to noise (SNR) calculations: A) Noise power density in bins of 1 Hz at the inner electrode  $d[n]$ , at the output of the DNF  $e[n]$  and at the output of the standard LMS based adaptive FIR filter. B) SNR in dB calculated with Eq. 19 at the inner electrode  $d[n]$  and the output  $e[n]$  of the DNF for every subject. C) SNR in dB calculated with Eq. 19 for the standard LMS based adaptive FIR filter for every subject. D) The SNR differences from C) and D) for DNF ( $\Delta\text{SNR}_{\text{DNF}} = 4.1 \pm 2.8$  dB) and FIR based LMS filter ( $\Delta\text{SNR}_{\text{LMS}} = 1.8 \pm 1.3$  dB).

$d[n]$  and the output from both the DNF and a standard LMS based adaptive FIR filter. The DNF filter achieves a nearly flat reduction of the noise to about  $0.1 \cdot 10^{-11} \text{ V}^2/\text{Hz}$  for frequencies above 10 Hz while the original noise from the inner electrode  $d[n]$  fluctuates widely between  $0.2 \cdot 10^{-11} \dots 0.8 \cdot 10^{-11} \text{ V}^2/\text{Hz}$ . The FIR filter tuned by LMS being a linear filter with just one layer also achieves a noise reduction but falls short by simply reducing the spectral components in a nearly proportional way and is not able to eliminate the noise peaks, for example at 35 Hz, 40 Hz or 45 Hz, but only reducing them.

The individual SNR changes between the different subjects are shown in panel B and C for DNF and LMS filters, respectively. It is evident that the worst SNR at  $-20\text{dB}$  can be improved most where strong EMG bursts from the jaw muscles are eliminated as shown in Fig. 2. For some subjects the improvement has been marginal and this might be due to poor electrode contact and thus little correlation between the inner and outer electrodes.

To test if the noise reduction has been statistically significant we calculated the SNR for every subject before and after filtering (in dB) to obtain the SNR improvement:

$$\Delta\text{SNR} = \text{SNR}_{\text{inner}} - \text{SNR}_{\text{DNF/LMS}} \quad (20)$$

Fig. 4D shows the SNR improvements for both the DNF and the LMS filter. Both

our new DNF ( $p = 0.000013$ ) and LMS tuned adaptive FIR filters ( $p = 0.000192$ ) significantly improved the SNR but the DNF is significantly better than the FIR LMS filter ( $p = 0.000026$ ).

## 4 Discussion

The least mean squares (LMS) technique to reduce noise in signals is well established (Widrow et al., 1975), where an FIR filter is trained to reduce the noise in a signal (Hayes, 1996) with the help of one or more reference signals (Jiang et al., 2019). This has been shown to be effective against EOG by using as a reference both the horizontal and vertical EOG to remove the artefacts from an EEG (He et al., 2004) but requires additional conventional electrodes placed above/below and left/right of the eyes. There have been various approaches of using neural networks to generate the signal (called here “remover”) which is used to eliminate the artefacts in the EEG signal (Islam et al., 2016). While we used a deep net with a non-linear activation function others used radial basis functions (Mateo et al., 2013) or functional link neural networks (FLNN) to generate non-linear decision boundaries with non-linear functional expansion (Jafarifarmand and Badamchizadeh, 2013). Even more computationally expensive is an approach where the shortcomings of the FLNN are reduced with the help of an adaptive neural fuzzy inference system (Hu et al., 2015). In contrast our deep network operates as a standard deep net and off-the-shelf optimised architectures are readily available.

Instead of employing an adaptive filter which receives a noise-reference one can also take the opposite approach and train a neural network with a clean EEG signal as a reference where after training the network then directly outputs the clean signal (Yang et al., 2018; Nguyen et al., 2012). This assumes that the clean EEG signal is available which is impossible for muscle noise as the subject cannot be paralysed. In order to overcome this problem one needs to add artefacts artificially to clean EEG data and then train the network to remove it (Nguyen et al., 2012). Given that a noise free EEG is not available the above neural network approaches rather rely on separate measurements of signal and noise which ranges from impractical to impossible. However, in our approach we use the readily available noise as a reference which can be measured with our compound electrode in real-time.

The mechanical EEG electrodes design is as old as the first EEG recordings (Umlauf, 1948) and the standard Ag/AgCl cup electrodes have been the main staple of EEG recordings ever since (McAdams, 2006). A major concern has always

been the resistance between electrode and skin (Schwab and Chock, 1953) which has an impact on the signal to noise ratio of the EEG. The electrode resistance has become even more of a concern with the advent of BCI and consumer EEG headbands which favour dry electrodes (Guger et al., 2012). Besides active electrodes (Xu et al., 2017) novel electrode designs promise to help reduce the electrode resistance (Krachunov and Casson, 2016; Velcescu et al., 2019) in particular by using spring contact probes (Nathan and Jafari, 2015; Liao et al., 2011). However, these electrode designs only improve the signal to noise ratio by a better skin/electrode contact but do not take into account the spatial distribution of signals versus noise which calls for compound electrodes.

The spatial distribution of the electrodes has been in particular investigated with the rise of brain computer interfaces (BCI) where often the user is actively using their muscles and thus creating a large amount of both EMG and movement artefacts (McFarland et al., 1997). It could be shown that the central average reference (CAR) and both small and large Laplacian montages (Besio et al., 2006) improve the signal to noise ratio. This has been shown for Electrocardiogram (ECG) (Garcia-Casado et al., 2019) by removing movement artefacts and for EEG (Aghaei-Lasboo et al., 2020). Common to all approaches is the approximation and optimisation of a 2D spatial Laplace operator (Besio et al., 2006; Makeyev et al., 2016; Makeyev, 2018). The more rings are employed at an optimal spacing the more efficient the operator will be. The calculation of the Laplacian is usually performed by the electrical summation of the EEG sources under each ring, digitised and then subtracted from each other. However, this assumes that every ring can perform a perfect analogue spatial averaging operation which is not the case in practice as electrode impedances will be inhomogeneous and changing over time. The analogue averaging over a ring can be overcome by measuring from a large number of electrodes from an EEG cap and then approximating the Laplace purely in software (Fitzgibbon et al., 2015) - but this is computationally expensive and if using a standard EEG cap, has its limitations in spatial resolution. On the other hand, the above discussed concentric ring electrode is the most feasible and practical hardware design (Besio et al., 2006), however, has the drawback of assuming perfect recording conditions only present in ideal biophysical models but not real setups. To overcome the shortcomings of hard wired computations based on ideal models we use an adaptive algorithm to account for the imperfect nature of the electrodes and the dynamic changes of electrode resistance over time, in particular when using dry electrodes. By highpass filtering the noise reference (i.e ring electrode) we can direct the learning algorithm towards the noise it should focus on

which was here EMG noise.

A particular area of concern is the choice of the adequate conductive electrode material. Bio-electrodes are in contact with the body and will in turn, be exposed to biological electrolytes which can, over time, cause oxidation of the electrode and degrade the electrode's quality (Lopez-Gordo et al., 2014; Manjakkal et al., 2019, 2020). It can be concluded that precious metals are the obvious choice for conductive material and many EEG electrodes utilise them to provide the electrode conductivity (Mathewson et al., 2017; Di Flumeri et al., 2019). Due to the cost of such metals, a superficial, thin coating is usually applied to a cheaper backing material (Gorecka and Makiewicz, 2019; Velcescu et al., 2019), to provide high conductivity, good chemical stability and structural support for the electrode, simultaneously minimising the cost (Manjakkal et al., 2018). The conductive layer selected for the design discussed in this paper was also Ag/AgCl and was selected due to its high conductivity (Velcescu et al., 2019), chemical and electrical stability (Lopez-Gordo et al., 2014) and relative manufacturing simplicity as it can be printed as an ink (Velcescu et al., 2019; Kalevo et al., 2020).

## **Conflict of Interest Statement**

B.P. is CEO of Glasgow Neuro LTD which manufactures the Attys DAQ board.

## **Author contributions**

B.P. and R.D. conceived the experiment(s), H.C. and L.M. conducted the experiment(s), S.D. and B.P. analysed the results. All authors reviewed the manuscript.

## **Funding**

This work was partly support by Engineering and Physical Sciences Research Council (EPSRC) through Engineering Fellowship for Growth - neuPRINTSKIN (EP/R029644/1)

## **Data Availability Statement**

The EEG dataset for this study can be found at <http://dx.doi.org/10.5525/gla.researchdata.1258>.

## References

- Aghaei-Lasboo, A., Inoyama, K., Fogarty, A. S., Kuo, J., Meador, K. J., Walter, J. J., et al. (2020). Tripolar concentric eeg electrodes reduce noise. *Clinical Neurophysiology* 131, 193–198. doi:10.1016/j.clinph.2019.10.022
- Ahmadi, A., Dehzangi, O., and Jafari, R. (2012). Brain-computer interface signal processing algorithms: A computational cost vs. accuracy analysis for wearable computers. In *2012 Ninth International Conference on Wearable and Implantable Body Sensor Networks*. 40–45. doi:10.1109/BSN.2012.19
- Besio, G., Koka, K., Aakula, R., and Dai, W. (2006). Tri-polar concentric ring electrode development for laplacian electroencephalography. *IEEE Transactions on Biomedical Engineering* 53, 926–933. doi:10.1109/tbme.2005.863887
- Britton, J. W., Frey, L. C., Hopp, J. L., Korb, P., Koubeissi, M. Z., Lievens, W. E., et al. (2016). *Electroencephalography (EEG): An Introductory Text and Atlas of Normal and Abnormal Findings in Adults, Children, and Infants* (American Epilepsy Society), 1 edn.
- [Dataset] Daryanavard, S., Porr, B., and Dahiya, R. (2022). Deep neuronal filter: EEG filter release. doi:10.5281/zenodo.6360675
- Delorme, A., Sejnowski, T., and Makeig, S. (2007). Enhanced detection of artifacts in eeg data using higher-order statistics and independent component analysis. *NeuroImage* 34, 1443–1449. doi:10.1016/j.neuroimage.2006.11.004
- Di Flumeri, G., Arico, P., Borghini, G., Sciaraffa, N., Di Florio, A., and Babiloni, F. (2019). The dry revolution: Evaluation of three different eeg dry electrode types in terms of signal spectral features, mental states classification and usability. *Sensors* 19, 1365. doi:10.3390/s19061365
- Fatourechi, M., Bashashati, A., Ward, R. K., and Birch, G. E. (2007). Emg and eeg artifacts in brain computer interface systems: A survey. *Clinical neurophysiology* 118, 480–494
- Fitzgibbon, S. P., DeLosAngeles, D., Lewis, T. W., Powers, D. M. W., Whitham, E. M., Willoughby, J. O., et al. (2015). Surface Laplacian of scalp electrical signals and independent component analysis resolve EMG contamination of electroencephalogram. *Int J Psychophysiol* 97, 277–84. doi:10.1016/j.ijpsycho.2014.10.006

- Fitzgibbon, S. P., Powers, D. M. W., Pope, K. J., and Clark, C. R. (2007). Removal of eeg noise and artifact using blind source separation. *Journal of clinical neurophysiology : official publication of the American Electroencephalographic Society* 24, 232–243. doi:10.1097/WNP.0b013e3180556926
- Garcia-Casado, J., Ye-Lin, Y., Prats-Boluda, G., and Makeyev, O. (2019). Evaluation of bipolar, tripolar, and quadripolar laplacian estimates of electrocardiogram via concentric ring electrodes. *Sensors* 19, 3780. doi:10.3390/s19173780
- Gorecka, J. and Makiewicz, P. (2019). The dependence of electrode impedance on the number of performed eeg examinations. *Sensors* 19, 2608. doi:10.3390/s19112608
- Green, R. M., Messick, W. J., Ricotta, J. J., Charlton, M. H., Satran, R., McBride, M. M., et al. (1985). Benefits, shortcomings, and costs of EEG monitoring. *Ann. Surg.* 201, 785–92. doi:10.1097/00000658-198506000-00017
- Guger, C., Krausz, G., Allison, B. Z., and Edlinger, G. (2012). Comparison of dry and gel based electrodes for p300 brain-computer interfaces. *Front Neurosci* 6, 60. doi:10.3389/fnins.2012.00060
- Hayes, M. (1996). *Statistical Digital Signal Processing and Modeling* (John Wiley & Sons)
- He, P., Wilson, G., and Russell, C. (2004). Removal of ocular artifacts from electroencephalogram by adaptive filtering. *Medical and biological engineering and computing* 42, 407–412
- Henry, J. C. (2006). Electroencephalography: basic principles, clinical applications, and related fields. *Neurology* 67, 2092–2092
- Hu, J., sheng Wang, C., Wu, M., xiao Du, Y., He, Y., and She, J. (2015). Removal of eeg and emg artifacts from eeg using combination of functional link neural network and adaptive neural fuzzy inference system. *Neurocomputing* 151, 278 – 287. doi:https://doi.org/10.1016/j.neucom.2014.09.040
- Islam, M. K., Rastegarnia, A., and Yang, Z. (2016). Methods for artifact detection and removal from scalp eeg: A review. *Neurophysiologie Clinique/Clinical Neurophysiology* 46, 287 – 305. doi:https://doi.org/10.1016/j.neucli.2016.07.002

- Jafarifarmand, A. and Badamchizadeh, M. A. (2013). Artifacts removal in eeg signal using a new neural network enhanced adaptive filter. *Neurocomputing* 103, 222 – 231. doi:<https://doi.org/10.1016/j.neucom.2012.09.024>
- Jiang, X., Bian, G.-B., and Tian, Z. (2019). Removal of Artifacts from EEG Signals: A Review. *Sensors (Basel)* 19. doi:10.3390/s19050987
- Jirayucharoensak, S., Israsena, P., Pan-ngum, S., and Hemrungronj, S. (2013). Online eeg artifact suppression for neurofeedback training systems. In *The 6th 2013 Biomedical Engineering International Conference (IEEE)*, 1–5
- Jirayucharoensak, S., Israsena, P., Pan-Ngum, S., Hemrungronj, S., and Maes, M. (2019). A game-based neurofeedback training system to enhance cognitive performance in healthy elderly subjects and in patients with amnesic mild cognitive impairment. *Clinical interventions in aging* 14, 347–360. doi:10.2147/CIA.S189047
- Kalevo, L., Miettinen, T., Leino, A., Kainulainen, S., Korkalainen, H., Myllymaa, K., et al. (2020). Effect of sweating on electrode-skin contact impedances and artifacts in eeg recordings with various screen-printed ag/agcl electrodes. *IEEE Access* 8, 50934–50943. doi:10.1109/access.2020.2977172
- Kher, R. and Gandhi, R. (2016). Adaptive filtering based artifact removal from electroencephalogram (eeg) signals. In *2016 International Conference on Communication and Signal Processing (ICCSP) (IEEE)*, 0561–0564
- Krachunov, S. and Casson, A. (2016). 3d printed dry eeg electrodes. *Sensors* 16, 1635. doi:10.3390/s16101635
- Liao, L.-D., Wang, I.-J., Chen, S.-F., Chang, J.-Y., and Lin, C.-T. (2011). Design, fabrication and experimental validation of a novel dry-contact sensor for measuring electroencephalography signals without skin preparation. *Sensors (Basel)* 11, 5819–34. doi:10.3390/s110605819
- Lopez-Gordo, M., Sanchez-Morillo, D., and Valle, F. (2014). Dry eeg electrodes. *Sensors* 14, 12847–12870. doi:10.3390/s140712847
- Makeyev, O. (2018). Solving the general inter-ring distances optimization problem for concentric ring electrodes to improve laplacian estimation. *BioMedical Engineering OnLine* 17. doi:10.1186/s12938-018-0549-6

- Makeyev, O., Ding, Q., and Besio, W. G. (2016). Improving the accuracy of laplacian estimation with novel multipolar concentric ring electrodes. *Measurement* 80, 44–52. doi:10.1016/j.measurement.2015.11.017
- Manjakkal, L., Dang, W., Yogeswaran, N., and Dahiya, R. (2019). Textile based potentiometric electrochemical ph sensor for wearable applications. *Biosensors*
- Manjakkal, L., Dervin, S., and Dahiya, R. (2020). Flexible potentiometric ph sensors for wearable systems. *RSC Advances* 10, 8594–8617
- Manjakkal, L., Sakthivel, D., and Dahiya, R. (2018). Flexible printed reference electrodes for electrochemical applications. *Advanced Materials Technologies* 3
- Mateo, J., Torres, A. M., and García, M. A. (2013). Eye interference reduction in electroencephalogram recordings using a radial basis function. *IET Signal Processing* 7, 565–576
- Mathewson, K. E., Harrison, T. J. L., and Kizuk, S. A. D. (2017). High and dry? Comparing active dry EEG electrodes to active and passive wet electrodes. *Psychophysiology* 54, 74–82. doi:10.1111/psyp.12536
- McAdams, E. (2006). *Bioelectrodes* (American Cancer Society). doi:10.1002/0471732877.emd013
- McFarland, D., McCane, L., David, S., and Wolpaw, J. (1997). Spatial filter selection for eeg-based communication. *Electroencephalography and Clinical Neurophysiology* 103(3), 389–394
- McMenamin, B. W., Shackman, A. J., Maxwell, J. S., Bachhuber, D. R. W., Koppenhaver, A. M., Greischar, L. L., et al. (2010). Validation of ica-based myogenic artifact correction for scalp and source-localized eeg. *NeuroImage* 49, 2416–2432. doi:10.1016/j.neuroimage.2009.10.010
- [Dataset] Munoz Bohollo, L. and Porr, B. (2022). EEG and P300 database to determine the signal to noise ratio during a variety of realistic tasks. doi:10.5525/gla.researchdata.1258
- Nathan, V. and Jafari, R. (2015). Design Principles and Dynamic Front End Re-configuration for Low Noise EEG Acquisition With Finger Based Dry Electrodes. *IEEE Trans Biomed Circuits Syst* 9, 631–40. doi:10.1109/TBCAS.2015.2471080

- Nguyen, H.-A. T., Musson, J., Li, F., Wang, W., Zhang, G., Xu, R., et al. (2012). Eeg artifact removal using a wavelet neural network. *Neurocomputing* 97, 374–389
- Nordin, A. D., Hairston, W. D., and Ferris, D. P. (2019). Human electrocortical dynamics while stepping over obstacles. *Sci Rep* 9, 4693. doi:10.1038/s41598-019-41131-2
- Rohaizad, N., Mayorga-Martinez, C. C., Novotny, F., Webster, R. D., and Pumera, M. (2019). 3d-printed ag/agcl pseudo-reference electrodes. *Electrochemistry Communications* 103, 104–108. doi:10.1016/j.elecom.2019.05.010
- Schwab, R. S. and Chock, Y. C. (1953). A circuit for checking both electrode continuity and resistance during EEG recording. *Electroencephalogr Clin Neurophysiol* 5, 447–9. doi:10.1016/0013-4694(53)90089-3
- Suarez-Perez, A., Gabriel, G., Rebollo, B., Illa, X., Guimerà-Brunet, A., Hernández-Ferrer, J., et al. (2018). Quantification of Signal-to-Noise Ratio in Cerebral Cortex Recordings Using Flexible MEAs With Co-localized Platinum Black, Carbon Nanotubes, and Gold Electrodes. *Frontiers in Neuroscience* 12. doi:10.3389/fnins.2018.00862
- Umlauf, C. W. (1948). A Simplified Basal Electrode for Routine EEG Use. *Science* 107, 121. doi:10.1126/science.107.2770.121
- Velcescu, A., Lindley, A., Cursio, C., Krachunov, S., Beach, C., Brown, C. A., et al. (2019). Flexible 3D-Printed EEG Electrodes. *Sensors (Basel)* 19. doi:10.3390/s19071650
- Widrow, B., Glover, J., McCool, J., Kaunitz, J., Williams, C., Hearn, R., et al. (1975). Adaptive noise cancelling: Principles and applications. *Proceedings of the IEEE* 63, 1692–1716. doi:10.1109/PROC.1975.10036
- Xu, J., Mitra, S., Hoof, C. V., Yazicioglu, R. F., and Makinwa, K. A. A. (2017). Active Electrodes for Wearable EEG Acquisition: Review and Electronics Design Methodology. *IEEE Rev Biomed Eng* 10, 187–198. doi:10.1109/RBME.2017.2656388
- Yang, B., Duan, K., Fan, C., Hu, C., and Wang, J. (2018). Automatic ocular artifacts removal in eeg using deep learning. *Biomedical Signal Processing and Control* 43, 148 – 158. doi:https://doi.org/10.1016/j.bspc.2018.02.021